

# Keypoints-Based Deep Feature Fusion for Cooperative Vehicle Detection of Autonomous Driving

Yunshuang Yuan<sup>1</sup>, Hao Cheng<sup>1</sup> and Monika Sester<sup>1</sup>

**Abstract**—Sharing collective perception messages (CPM) between vehicles is investigated to decrease occlusions, so as to improve perception accuracy and safety of autonomous driving. However, highly accurate data sharing and low communication overhead is a big challenge for collective perception, especially when real-time communication is required among connected and automated vehicles. In this paper, we propose an efficient and effective keypoints-based deep feature fusion framework, called FPV-RCNN, for collective perception, which is built on top of the 3D object detector PV-RCNN. We introduce a bounding box proposal matching module and a keypoints selection strategy to compress the CPM size and solve the multi-vehicle data fusion problem. Compared to a bird’s-eye view (BEV) keypoints feature fusion, FPV-RCNN achieves improved detection accuracy by about 14% at a high evaluation criterion (IoU 0.7) on a synthetic dataset COMAP dedicated to collective perception. Also, its performance is comparable to two raw data fusion baselines that have no data loss in sharing. Moreover, our method also significantly decreases the CPM size to less than 0.3KB, which is about 50 times smaller than the BEV feature map sharing used in previous works. Even with a further decreased number of CPM feature channels, i.e., from 128 to 32, the detection performance only drops about 1%. The code of our method is available at [https://github.com/YuanYunshuang/FPV\\_RCNN](https://github.com/YuanYunshuang/FPV_RCNN).

## I. INTRODUCTION

Understanding the surrounding environment is one of the most important tasks of autonomous driving, especially for those automated vehicles (AV) driving in complex real-world situations. Such an AV is normally equipped with different sensors like cameras, LiDARs, and Sonars in order to sense the world [1]. However, perceiving the environment only using the data collected by these sensors mounted on a single ego vehicle has many limitations, such as occlusion, limited sensor observation range and noise. In this regard, cooperative perception based on connected and automated vehicles (CAV) can effectively mitigate these problems by sharing sensed information collected from different view directions of multiple AVs in a network, the so-called agent network. The perceived information is shared among vehicles via Collective Perception Messages (CPM). This way, the accuracy and reliability requirements of the sensors on each vehicle can be relaxed, and therefore the cost of each AV is lowered as well [2]. However, the challenging part of cooperative perception is to define the information to be shared and the method of fusing the shared information via a limited communication network bandwidth. Hence, the goal

<sup>1</sup>Yunshuang Yuan, Hao Cheng and Monika Sester are with the Institute of Cartography and Geo-informatics, Leibniz University Hannover, Germany {firstname.lastname}@ikg.uni-hannover.de.

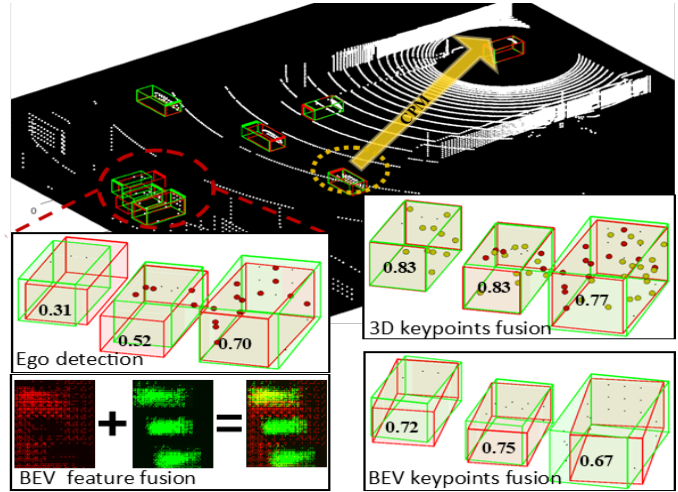


Fig. 1. Detection result of an exemplary frame with two CAVs. The vehicle in the yellow dashed circle shares CPM to the ego vehicle (upper right). According to the IoUs (marked in the boxes) of predictions (red box) against the ground truth (green box), our proposed method of the 3D keypoints fusion outperforms the BEV keypoints fusion by a large margin for improving ego vehicle’s detection.

is to obtain the best perception performance with the least data transmission in the agent network.

High accurate data sharing and low communication overhead is still a bottleneck for cooperative vehicle detection demanding real-time communication in autonomous driving. In theory, sharing raw data gives the best performance because no information is lost. But this can easily congest the communication network with heavy data loads. In contrast, sharing the fully processed data, e. g., detected objects, needs fewer communication resources. Nevertheless, this method is very sensitive to the positioning error of the agents and hard to match the detected objects coming from different agents, especially those that are inaccurately detected by distant sensors. As a tradeoff, deep features can decrease the amount of data to be shared and at the same time maintain a relatively high performance of data fusion. However, the contracted bird’s-eye view (BEV) deep features maps that are learned by a Deep Neural Network (DNN) in previous works [3]–[5] are very sparse and can be further compressed to avoid redundancy. Moreover, due to the low resolution, fusing such feature maps may even fail to predict accurate bounding boxes. To this end, this paper proposes a more robust deep feature sharing and fusion strategy. PointNet [6] and point set abstraction [7] are used to aggregate the infor-

mation from multi-scale receptive field for the selected high accurate 3D points. These selected points with aggregated features are called keypoints and are shared and fused to generate more accurate detections. In comparison to the BEV keypoints fusion, with reduced communication overhead our 3D keypoints fusion still achieves higher detection accuracy. An example tested on the synthetic collective perception dataset COMAP [8] is shown in Fig. 1.

Our main contributions are summarized as follows.

- 1) We propose a 3D keypoints feature fusion scheme for cooperative vehicle detection to remedy the problem of low bounding box localization accuracy of the schemes that are based on the BEV feature fusion.
- 2) We introduce a matching and keypoint selection module to reduce the redundancy of shared deep features, so as to decrease the communication overhead.
- 3) Our proposed method not only outperforms the state-of-the-art method that uses BEV feature fusion for collective perception with a large margin but also reduces the CPM data size by a large scale.

## II. RELATED WORK

In general, cooperative perception can be achieved by means of Vehicle-to-Infrastructure (V2I) and Vehicle-to-Vehicle (V2V) communication. V2I communication offers the opportunity to exchange sensory information between an ego vehicle and the infrastructure. This helps the ego vehicle go beyond the limitations of its own perception system. A successful application is the so-called smart intersection [9], where information for the vehicle and pedestrian detection and tracking is shared via the BEV observation from the static cameras at the intersection to the vehicle. These cameras are easy to deploy, whereas their perceptions are limited to traffic scenarios at the specific intersection. In contrast, V2V communication is not limited to the defined location. In a CAV network, each vehicle can be seen as a node with multiple sensors, the sensed data can be shared among the vehicles at any place [10]. Our work focuses on V2V communication for object detection.

In V2V communication, different approaches are proposed to communicate the data in a CAV network. In this paper, we sort data fusion strategies as (1) raw data sharing, (2) fully processed data, such as detected objects, and (3) half-processed data. Raw data sharing though provides rich information for OD, it consumes large bandwidth and is not feasible for autonomous driving that requires real-time communication [4]. Contrary to raw data sharing, [11]–[13] propose to only share the detected objects for a more efficient communication. However, it is proven that this late fusion of fully processed data performs worse than either early raw data fusion or half-processed data [5].

In order to reduce communication consumption without a compromise of performance, sharing half-processed data is further explored. In an extreme case, objects mis-detected by all independent sensors can be detected after this data fusion. For example, instead of detected objects, Chen et al. [3] extends their previous work [13] by fusing voxel features

and deep features learned using a Deep Neural Network (DNN) for cooperative perception. Significant performance improvement has been shown on the real-world datasets KITTI [14] and T&J [13]. However, these datasets only contain a limited number of traffic scenarios, e.g., in a parking lot [13], and they are not dedicated to collective perception. This is because acquiring this type of real-world dataset is expensive and needs numerous hours of manual labeling to obtain ground truth information. Therefore, many recent works [4], [15] resort to synthetic data for a more comprehensive empirical study. Data generator and simulation tools e.g., CARLA and SUMO [16], not only can be manipulated to generate a large amount of realistic data in various traffic situations for cooperative perception, but also provide accurate ground truth information. In [4], the comparison of different data fusion strategies on a simulated point cloud dataset generated by CARLA indicates that both the raw data and deep feature fusion outperform the object-wise fusion by a big margin, especially when vehicle localization error is introduced. In addition, [5] also confirms that on the simulated dataset LiDARsim [15], sharing compressed deep feature maps achieves high accurate object detection while satisfying communication bandwidth requirements.

Despite the preliminary success of deep feature fusion, the shared feature maps still contain too much redundancy due to the fact of their sparsity. These deep features are highly abstract, which are difficult to be selected, compressed, and finally fused by a neural network. For example, [3]–[5] try to share intermediate feature maps for vehicle detection. It is found that this strategy is not robust in providing highly accurate bounding box predictions, because the shared feature maps are of low resolution, i.e.,  $8\times$  down-sampled from the raw data. Thus, in this paper, we investigate sharing only the selected keypoint features, aiming to further reduce the deep feature size while keeping the performance of object detection.

## III. METHOD

### A. Problem Formulation

We assume a hybrid traffic scenario, which contains both CAVs and unautomated vehicles, and formulate the collective perception problem in an ego-centric way. Within a communication range  $R_c$  of the ego-vehicle  $C_0$ ,  $N_v$  number of cooperative CAVs ( $\{C_1, C_2, \dots, C_{N_v}\}$ ) as well as the ego CAV have generated the point cloud set  $\mathbf{PC} = \{PC_0, PC_1, \dots, PC_{N_v}\}$  at time  $t$ . The bounding boxes (BBox) of the  $N_i$  vehicles detected based on  $PC_i$  are called proposals and notated as  $B_i = \{(b_j, s_j) \mid j = 1, \dots, N_i\}$ . Each instance in  $B_i$  is a pair that contains one detected vehicle  $b_j = (x, y, z, w, l, h, r)$  and its corresponding detection confidence  $s_j$ . In this notation,  $xyz$  indicates a BBox center in  $x$ -,  $y$ -, and  $z$ -axis,  $wlh$  the dimensions of width, length, and height, and  $r \in [-\pi, \pi]$  the orientation. In our proposed framework, the cooperative CAV  $C_i$  ( $1 \leq i \leq N_v$ ) generates and shares to the ego CAV  $C_0$  the CPM $_i$  that contains  $B_i$  and the selected and aggregated deep feature information  $F_i$  (see Sec. III-B.0.b). The ego CAV then

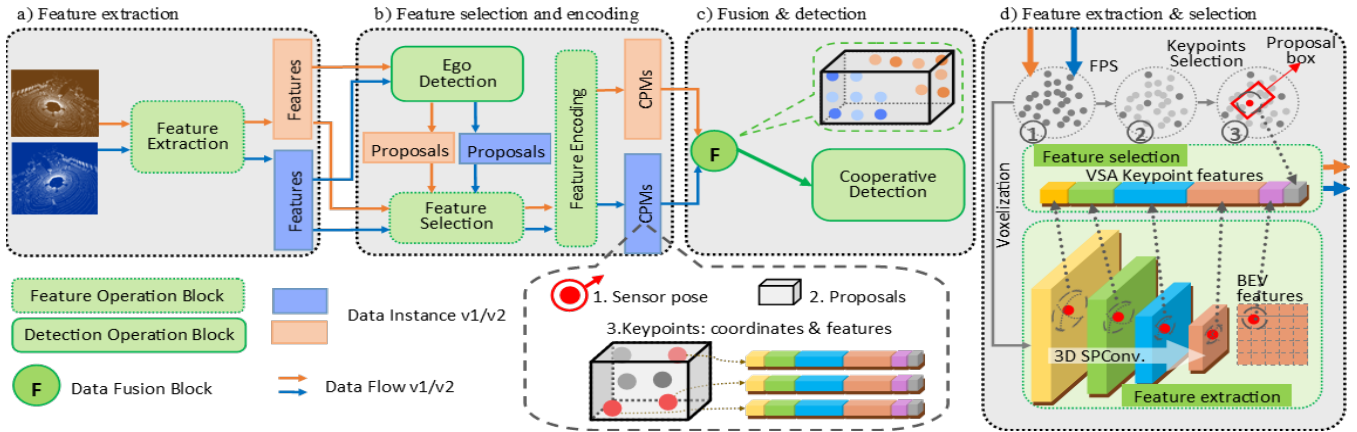


Fig. 2. An overview of the keypoints deep feature fusion framework (FPV-RCNN). Block a)-c) show the overall pipeline of the framework, while d) illustrates the details of the feature extraction and selection modules in block a) and b), and the gray dashed dialog box shows the CPMs.

fuses this information of the received CPMs with the local information and generates the final refined predictions.

### B. 3D Keypoints Deep Features Fusion

The fusion framework proposed is built based on the 3D object detector PV-RCNN [17], hence we term this framework as FPV-RCNN (Fusion PV-RCNN) and notate it as **3Dr** for simplicity. Here 3D stands for 3D keypoint features and **r** the RCNN head. Figure 2 demonstrates a fusion example of two CAVs, while it can be easily extended to arbitrary number of CAVs. Data flows of the two CAVs are color coded in blue and orange, respectively. We first extract deep features separately from the point clouds (Fig. 2a) and then select and encode the most important features for sharing (Fig. 2b). At last, the shared features are fused for the final detection (Fig. 2c).

*a) Feature extraction:* To extract the 3D features of point clouds, we adopt the voxel-based sparse CNN backbone network from [17] because of its high efficiency and accuracy. This network is demonstrated in the bottom of Fig. 2d. First, the raw point cloud is voxelized and then passed to a block of 3D sparse convolutions (3D SPConv.) [18], [19]. After the 3D SPConv., the original voxel features are encoded and  $8\times$  down-sampled to 3D deep features. In the end, the features from the last sparse convolution layer are further compressed to BEV features.

*b) Feature selection and encoding:* The ego-detection module adopts CIA-SSD [20] as the detection head. This is because CIA-SSD has a simple structure and can generate better proposals than the proposal generation module in two-stage detectors. This ego-detection module generates proposals  $B_i$ , and later these proposals are utilized for selecting feature points. It should be noted that in order to decrease the size of CPMs, only the feature points inside the proposals are selected, further encoded, and compressed to CPM format. The details of feature selection is shown in Fig. 2d. Furthest Points Sampling (FPS) is used to sample a pre-defined number of  $N_{\text{kpts}}$  evenly distributed sparse keypoints

(as shown from step ① to ②). These keypoints are then further reduced by only selecting the keypoints that are in the proposal BBoxes  $B_i$  (as shown from step ② to ③). Based on the selected keypoints, the Voxel Set Abstraction (VSA) module with the same parameters that are in [17] to aggregate deep features for each selected keypoint. The VSA module aggregates neighboring voxel-wise features of different resolutions and abstract levels for each keypoints using a PointNet [6]. The aggregated keypoint features are then encoded and compressed for generating CPM. As exemplified in the dialog box of Fig. 2, for the point cloud  $PC_i$ , we compose the  $CPM_i$  using the sensor pose of CAV  $C_i$ , proposals  $B_i$ , and coordinates & features of keypoints  $F_i$ .

*c) Fusion and detection:* In the fusion step, the ego-vehicle transforms all received proposal boxes and keypoints into the same local coordinate system. These transformed proposals are then clustered and merged via algorithm 1:

- If the IoU of two proposals in set  $\mathcal{B}$  is above a pre-defined threshold (e.g., 0.3), they are clustered into the same subsets  $C_k$  (Line 1-5).
- In each  $C_k$ , we first align the direction  $r_i$  of each BBox  $b_i$  to the dominant direction of all BBoxes in this cluster in order to prevent erroneous orientation merging caused by conflicting BBox directions (Line 8-13).
- We merge the BBoxes in each cluster to one single proposal by weighing the BBox parameters with their prediction confidence  $s_i$  (Line 14-16).
- After merging the BBoxes in each cluster, we end up with  $K$  merged proposals which are collected in the set  $M$ .

As shown in Fig. 2c, the merged proposal (black box) of set  $M$  is refined by aggregating the neighboring keypoints (darker colored points) coming from different CPMs. This aggregation is achieved by a VSA-based RoI-grid pooling module originally proposed in [17]. It divides the proposal box into regular grids and summarizes the neighboring keypoints information for each grid center. The aggregated grid features are then stretched to a vector and fed to the fully

---

**Algorithm 1** Cooperative BBox Matching

---

**Ensure:**  $\mathcal{B} = B_1 \cup B_2 \cup \dots \cup B_{N_v}$ , cluster set  $\mathcal{C} = \emptyset$ , cluster index  $k = 1$ ,  $\text{iou}_{\text{thr}} = 0.3$ , merged proposal set  $M = \emptyset$ .

```
1: while  $\mathcal{B} \neq \emptyset$  do
2:   Select one BBox  $b$  from set  $\mathcal{B}$ 
3:    $C_k = \{(b', s') | (b', s') \in \mathcal{B}, \text{IoU}(b', b) > \text{iou}_{\text{thr}}\}$ 
4:    $\mathcal{B} \leftarrow \mathcal{B} \setminus C_k$ ,  $\mathcal{C} \leftarrow \mathcal{C} \cup \{C_k\}$ ,  $k = k + 1$ 
5: end while
6: for each  $C_k \subset \mathcal{C}$  do
7:    $I \leftarrow \{i | (s_i, b_i) \in C_k\}$ 
8:    $r_{\text{max}} = \text{argmax}_r S$ , where  $S = \{s_i | i \in I\}$ 
9:    $S_{\text{dir1}} = \sum_{I_1} s_{i1}$ ,  $I_1 = \{i1 | |r_{i1} - r_{\text{max}}|_a > \frac{\pi}{2}, i1 \in I\}$ 
10:   $S_{\text{dir2}} = \sum_{I_2} s_{i2}$ ,  $I_2 = \{i2 | |r_{i2} - r_{\text{max}}|_a \leq \frac{\pi}{2}, i2 \in I\}$   $\triangleright$ 
     $|\cdot|_a$  is the angle difference and normalized to  $[0, \pi]$ 
11:   $I_{\text{max}} \leftarrow \text{argmax}_{\{I_1, I_2\}} (S_{\text{dir1}}, S_{\text{dir2}})$ 
12:  for all  $i \in I_{\text{max}}$  do  $r_i \leftarrow r_i + \pi$ 
13:  end for
14:   $s_{i, \text{norm}} = s_i / \sum_j s_j$ ,  $i, j \in I$ 
15:   $m_* = \sum_i b_{i*} \cdot s_{i, \text{norm}}$ ,  $* \in \{x, y, z, w, l, h\}$ ,  $i \in I$ 
16:   $m_r = \arctan2(\sum_i s_{i, \text{norm}} \cdot \sin r_i, \sum_i s_{i, \text{norm}} \cdot \cos r_i)$ ,  $i \in I$ 
17:   $M \leftarrow M \cup \{(m_x, m_y, m_z, m_l, m_w, m_h, m_r)\}$ 
18: end for
19: return  $M$ 
```

---

connected layers to generate the final cooperative detection result. This result not only contains a binary classification between positive and negative proposals, but also the proposal box refinement regression. Other than in [17], the batch normalization (BN) [21] in the fully connected layers is replaced by a dropout [22] so that the batch size can be set to one in training time.

Similar to [5] for a fair comparison of the CPM size by sharing original feature maps and keypoint features, 3D data compressor Draco [23] is applied to compress the encoded CPM features. For both feature formats, we first write the 2D points of feature maps or the 3D keypoints to PLY [24] file format and then compress this file with Draco.

## IV. EXPERIMENTS

### A. Dataset

To evaluate the performance of the proposed method, we use a synthetic cooperative perception dataset called COMAP [8], which is simulated by CARLA [25] and SUMO [16]. Despite many existing real-world datasets like KITTI [14], nuScenes [26], and Waymo [27], they are more suited for ego-perception, whereas collective perception requires that multiple CAVs should observe the same scenario at the same time with enough overlaps of field-of-view (FOV). On the contrary, the synthetic dataset containing various realistic cooperative vehicle scenarios with accurate ground truth information is easy to acquire and needs no more manual work of data labelling. In addition, the lack of benchmark datasets leads the difficulty to comparing the

performance of different fusion methodologies. Hence, in this paper, we follow many other works [4], [5], [15] to use such a synthetic dataset for the empirical studies.

In total, there are 7788 frame samples in COMAP—4155 frames for training and 3633 frames for testing. Each frame contains the point cloud of an ego vehicle, the point clouds of the cooperative vehicles in the ego vehicle’s communication range within 40 m, and the corresponding ground truth (GT) BBoxes for each CAV. In the simulation, the GT BBoxes of all vehicles are known, including the ones that are outside the valid detection range or on other parallel roads. We only select the GT BBoxes that are in the driving distance (the shortest road distance the observer vehicle needs to drive to the location of an observed vehicle) to evaluate the collective perception framework. This distance is a hyperparameter that can be changed, in this study it is set  $R = 57.6$  m for a sufficient gap to ensure the safety between vehicles. For communication efficiency, only up to four point clouds of the cooperative vehicles are loaded. To facilitate the feature fusion step and avoid a big performance drop for the object detection caused by the LiDARs mounted on many vehicles of different heights, all the point clouds are aligned to the world z-coordinate, including height and orientation on the road plane. After this alignment, all the point clouds are filtered by the same range  $R$  on the x-y plane and the height range  $[-0.1, 3.9]$  m. During training, the occluded GT BBoxes with no observed reflected points are removed. In the end, the pre-processed point clouds are voxelized to a size of 0.1 m before they are fed to the DNNs in the framework (see Fig. 2).

### B. Comparative Models and Evaluation Metrics

a) *BEV feature fusion:* Since deep BEV features are the most commonly used fusion method (see Sec. II), we also implement such a fusion model to compare it with our proposed model **3Dr**. However, different from previous works, we only select features that are inside the proposals  $B_i$  for sharing to ensure a fair comparison between BEV and 3D feature fusion with a similar magnitude of CPM size. We denote this comparative model as **BEVs**, where s stands for the SSD detection head of CIA-SSD.

The pipeline of this method is compatible with the one depicted in Fig. 2(a-c). The details of the modules that are different from **3Dr** are shown in Fig. 3. The BEV features generated by feature extraction are passed to a Spatial-Semantic Feature Aggregation (SSFA) [20] module, which can extract more robust features for generating accurate predictions. This feature map is further encoded and compressed by two convolutional layers and then selected by the proposals  $B_i$ . In addition to the selected BEV keypoints, the CPMs in this case also contain the sensor pose but no proposals, because they are not needed for the single-stage detector. In the fusion step, the shared feature maps are first up-sampled to a higher resolution by several transposed convolution layers and then merged by a summation of weighted feature maps. The weights are automatically adaptable as they are learned by a convolutional layer. The merged feature maps



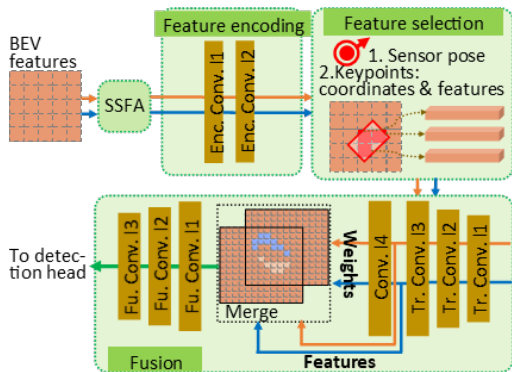


Fig. 3. An overview of BEV deep feature fusion

are then further fused and contracted by three convolutional layers to the detection resolution for the final detection.

*b) Baseline:* We take the raw data fusion strategy as a baseline. This strategy avoids any data loss during sharing, hence more likely to perform the best. Namely, two corresponding raw data fusion networks are taken as baselines—one for BEV-keypoints fusion (noted as **RDs**) and another for 3D-keypoints fusion (noted as **RDr**). **RDs** takes CIA-SSD as the base object detector. Its raw data fusion framework is adopted from [8] and is a part of the FPV-RCNN framework that only contains the feature extraction and ego-detection module. For **RDr**, we add VSA and RCNN (RoI-grid pooling and detection head) module to **RDs** in order to refine the proposals as similar to **3Dr** as possible.

*c) Evaluation Metrics:* All test results are evaluated with mean Average Precision (mAP) defined by the Area Under Precision-Recall Curve (PR-AUC). To evaluate the detection performance of different localization accuracy, we use different IoU thresholds (0.3, 0.5, 0.7) for counting the positive detections.

### C. Experimental Setups

*a) Training setting:* The targets for training are generated relative to the pre-defined anchors. For **RDs** and **BEVs** and the ego detection of **RDr** and **3Dr**, we generate two anchors corresponding to rotations 0 and  $\pi/2$  on each location of the  $8 \times 8$  down-sampled feature maps. The anchors are of [4.41, 1.98, 1.64]m in length, width and height. The anchor is defined as positive if it has an IoU against a GT BBox over 0.6, negative if under 0.45, and ignored otherwise for the classification. For the cooperative detection of **RDr** and **3Dr**, we generate targets relative to the merged proposals by the ego detection (see Algorithm 1). But a single IoU threshold of 0.3 is used to separate the positive ( $\geq 0.3$ ) and negative ( $< 0.3$ ) samples for the classification. For ego detection, we supervise the prediction results of all the incoming point clouds **PC** (see Sec. III-A) separately. However, for the cooperative perception, we only supervise the detection results from the perspective of the ego point cloud.

The same loss functions and the parameters for SSD head from the original work [20] are adopted for object

classification. But positive and negative samples are weighted differently, i.e., 50 vs. 1, to prevent the network from classifying all samples as negative. For the RCNN head, a binary cross-entropy loss is used for classification and smooth  $L_1$ -loss for regression. They are normalized over all samples. Since the CAVs also share their own poses with each other, we also add the GT BBoxes of the ego vehicle and all selected cooperative vehicles to the detection before feeding them to the Non-Maximum-Suppression (NMS). The thresholds for classification scores and NMS IoUs are set to 0.3 and 0.01, respectively, and kept the same in testing phase.

We run all the experiments only on a single Nvidia 1080Ti GPU to simulate a restricted computational resource in an AV. **RDs** is trained from scratch for 50 epochs with a batch size of 8 frames. The trained weights of this network are then used for initializing the weights of the feature extraction and ego detection module in **RDr**, **BEVs**, and **3Dr**. These three networks are then further fine-tuned for 10 epochs with a batch size of 4 for **RDr** and 1 for the other two. The Adam optimizer (coefficients of 0.95&0.999) is applied to optimize the losses by stochastic gradient descent. Its learning rate and decay both are set to  $1e^{-4}$ . We provide the detailed setting at our repository for reproducing our models.

*b) Test setting:* Different numbers of cooperative vehicles are tested for analyzing the performance of cooperative perception. This is done by fixing the number of cooperative vehicles  $N_v$  in each test run. Namely,  $N_v$  varies from 0, 2 to 4. In each run, only the frames having at least  $N_v$  cooperative point clouds are selected as a test set for evaluation. If there are more than  $N_v$  cooperative point clouds, we randomly select  $N_v$  out of them to simulate the random geometric distribution of CAVs.

Moreover, different CPM feature channels are analyzed for the keypoints feature fusion. We set CPM feature channels to 128 to compare BEV and 3D keypoints fusion under the condition of no information loss during the CPM compression process. To further investigate the possibility of decreasing the size of CPMs in the **3Dr** framework, we conduct a series of experiments by setting different  $N_{kpts}$  for FPS (2048 and 1024) and different CPM feature encoding channels  $N_{ch}$  (128, 64, and 32).

## V. RESULT AND EVALUATION

### A. Comparison of Prediction Performance

Table I shows the mAP scores of the baselines (in gray cell) and the fusion models. With cooperative vehicles ( $N_v > 0$ ), compared to the best performed RD fusion baselines (bold font in gray cell), both BEV-fusion and 3D-fusion have an acceptable small performance drop at the low IoU threshold (0.3). For example, when there are only two cooperative vehicles, the mAP of **BEVs** at IoU = 0.3 drops 1.22% while that of 3D-fusion only drops 0.73%. However, as IoU threshold increases to 0.5, the gap between **BEVs** and **RDs** increases rapidly. At IoU = 0.7, the gap between them even increases to 13.71%. In contrast, the performance gaps between **3Dr** and its baseline **RDr** are smaller and remain consistent. It is worth noting that the performance of **3Dr**

TABLE I Mean AP of different fusion models (in %)

IoU	$N_v$	<b>RDs</b>	<b>RDr</b>	<b>BEVs</b>	Ours ( <b>3Dr</b> )
0.3	0	<b>82.45</b>	78.95	<b>83.64</b>	76.11
	2	<b>95.74</b>	94.85	94.52	<b>95.01</b>
	4	<b>98.40</b>	98.07	97.20	<b>97.95</b>
0.5	0	<b>79.85</b>	77.33	<b>81.06</b>	74.29
	2	<b>94.74</b>	94.07	92.27	<b>94.35</b>
	4	<b>97.80</b>	97.68	94.33	<b>97.53</b>
0.7	0	66.13	<b>67.24</b>	<b>70.09</b>	65.97
	2	89.30	<b>89.63</b>	75.59	<b>90.08</b>
	4	94.86	<b>95.18</b>	78.46	<b>95.04</b>

even overtakes that of **RDs** with a small mAP gain at IoU = 0.7. This implies that the additional RCNN-head helps improve the localization accuracy of the BBoxes at lower IoU thresholds, but not the recall of the BBoxes. On the other hand, the RoI-grid pooling can better aggregate the 3D keypoints features learned from point cloud for high accurate BBox predictions. In other words, compared to **BEVs**, our model is more suitable for feature fusion of cooperative object detection with respect to high accurate and reliable BBox predictions.

Nevertheless, when there are no cooperative vehicles, our **3Dr** performs much worse than the other two baselines. This is because these self-dependent detection results are generated only by the feature extraction and ego-detection module. The weights of these two modules are fine-tuned during the training of the whole BEV and 3D fusion framework. This indicates that **BEVs** tends to learn features that are more helpful for detection task on a single point cloud. Thus, it overfits in such a configuration with better performance than that of the more generalized **RDs** (e.g., 70.09% vs. 66.13% at IoU = 0.7). In contrast, **3Dr** focuses on learning features that are useful for the later fusion, and therefore are counter-affected by the original pre-trained weights for non-cooperative detection. It should be noted that this issue can be circumvented by loading different pre-trained weights according to the requirements in real applications.

### B. FPV-RCNN Performance with Variate CPM Sizes

Table II shows the results of FPV-RCNN (**3Dr**) with different CPM encoding parameters.  $N_{kpts}$  stands for the number of keypoints for FPS and  $N_{ch}$  stands for the number of channels for encoding the CPM features. Besides, the results are evaluated with two different numbers of cooperative vehicles ( $N_v = \{2, 4\}$ ). In general, the better performance is mostly associated with a larger  $N_{kpts}$  and all best mAP scores (bold blue font) appear when  $N_v = 2048$ . But for a specific IoU and  $N_v$ , the performance only varies within a range of less than 1% for different  $N_{ch}$ . Interestingly, in most cases the best mAP even appears at the smallest  $N_{ch}$  (bold font).

Furthermore, we compare the CPM sizes of the compressed deep features averaged over all CPMs and CAV numbers. Figure 4 gives a quantitative comparison between BEV and the keypoints feature sharing we proposed (noted as 3D with a different number of keypoints). It can be seen that the average CPM size of the compressed keypoints

TABLE II Performance of FPV-RCNN (**3Dr**) with different number of keypoints and CPM encoding channels (in %)

IoU↓	$N_v \rightarrow$	$N_{ch} \downarrow, N_{kpts} \rightarrow$	2		4	
			2048	1024	2048	1024
0.3	128	128	95.01	94.69	97.95	97.32
		64	94.58	95.08	97.97	97.96
		32	<b>95.25</b>	<b>95.12</b>	<b>98.13</b>	<b>98.01</b>
0.5	128	128	94.35	93.89	97.53	96.76
		64	94.01	<b>94.31</b>	97.58	<b>97.53</b>
		32	<b>94.78</b>	94.28	<b>97.81</b>	97.49
0.7	128	128	<b>90.08</b>	<b>89.72</b>	<b>95.04</b>	94.18
		64	89.60	89.67	94.95	94.56
		32	89.39	<b>89.72</b>	94.76	<b>94.92</b>

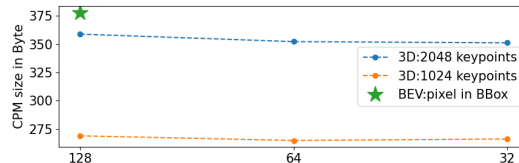


Fig. 4. CPM size comparison

features is decreased to around 0.3KB, which is about 50 times smaller than the CPM generated by compressing the whole feature maps (ca. 14KB). With the same number of feature channels ( $N_{ch} = 128$ ), 3D keypoints fusion transmits less data than the BEV keypoints fusion but achieves an enhanced performance by a big margin (95.04% vs. 78.46%, see Table I). Besides, **3Dr** also generates CPMs with sizes in the same order of magnitude as the object-based standardized CPM [28] evaluated in a low traffic density scenario by [29].

These observations above indicate that our proposed framework is relatively stable against the variation of the CPM feature encoding size. Hence, if the communication network is not fully consumed and the wireless network can handle larger CPMs, it is preferred to increase  $N_{kpts}$  rather than increase the feature encoding channels. On the other hand, as a big advantage, if the communication network is already heavily loaded, the CPMs can be compressed as small as possible with only a slight performance drop.

## VI. CONCLUSION

In this paper, we proposed an efficient framework, called FPV-RCNN, for point cloud-based cooperative vehicle detection of autonomous driving. The framework takes PV-RCNN [17] as the base network of object detection for cooperative perception scenarios by introducing a bounding box proposal matching and fusion module, as well as a keypoints selection module. The comparison to a 2D BEV feature fusion on a simulated dataset COMAP [8] shows that our method not only improves the performance of cooperative vehicle detection by a big margin but also significantly decreases the data transmission load in the CAV network for real-time communication. In future work, we plan to extend our framework to vulnerable road users, such as pedestrians and cyclists, and evaluate our method in real-world cooperative driving scenarios.

## REFERENCES

- [1] C. Premebida, R. Ambrus, and Z.-C. Marton, "Intelligent robotic perception systems," in *Applications of Mobile Robots*, 2019, pp. 111–127.
- [2] M. Shan, K. Narula, R. Wong, S. Worrall, M. Khan, P. Alexander, and E. Nebot, "Demonstrations of cooperative perception: Safety and robustness in connected and automated vehicle operations," *Sensors (Basel, Switzerland)*, vol. 21, 2021.
- [3] Q. Chen, X. Ma, S. Tang, J. Guo, Q. Yang, and S. Fu, "F-cooper: Feature based cooperative perception for autonomous vehicle edge computing system using 3d point clouds," in *Proceedings of the 4th ACM/IEEE Symposium on Edge Computing*. Association for Computing Machinery, 2019, p. 88–100.
- [4] E. E. Marvasti, A. Raftari, A. E. Marvasti, Y. P. Fallah, R. Guo, and H. Lu, "Feature sharing and integration for cooperative cognition and perception with volumetric sensors," in *arXiv e-prints*, Nov. 2020, p. arXiv:2011.08317.
- [5] T.-H. Wang, S. Manivasagam, M. Liang, B. Yang, W. Zeng, and R. Urtasun, "V2VNet: vehicle-to-vehicle communication for joint perception and prediction," in *Computer Vision - ECCV 2020 - 16th European Conference, Proceedings, Part II*, vol. 12347. Springer, 2020, pp. 605–621.
- [6] C. R. Qi, H. Su, K. Mo, and L. J. Guibas, "Pointnet: Deep learning on point sets for 3d classification and segmentation," in *2017 IEEE Conference on Computer Vision and Pattern Recognition*. IEEE Computer Society, 2017, pp. 77–85.
- [7] C. R. Qi, L. Yi, H. Su, and L. J. Guibas, "Pointnet++: Deep hierarchical feature learning on point sets in a metric space," in *Advances in Neural Information Processing Systems*, ser. NIPS'17. Curran Associates Inc., 2017, pp. 5099–5108.
- [8] Y. Yuan and M. Sester, "COMAP: A synthetic dataset for collective multi-agent perception of autonomous driving," *The International Archives of the Photogrammetry, Remote Sensing and Spatial Information Sciences*, vol. XLIII-B2-2021, pp. 255–263, 2021.
- [9] S. Yang, E. Bailey, Z. Yang, J. Ostrometzky, G. Zussman, I. Seskar, and Z. Kostic, "COSMOS smart intersection: Edge compute and communications for bird's eye object tracking," in *2020 IEEE International Conference on Pervasive Computing and Communications Workshops (PerCom Workshops)*, 2020, pp. 1–7.
- [10] T. Niels, N. Mitrovic, K. Bogenberger, A. Stevanovic, and R. L. Bertini, "Smart intersection management for connected and automated vehicles and pedestrians," in *2019 6th International Conference on Models and Technologies for Intelligent Transportation Systems (MT-ITS)*, 2019, pp. 1–10.
- [11] C. Allig and G. Wanielik, "Alignment of perception information for cooperative perception," in *2019 IEEE Intelligent Vehicles Symposium*. IEEE, 2019, pp. 1849–1854.
- [12] A. Miller, K. Rim, P. Chopra, P. Kelkar, and M. Likhachev, "Cooperative perception and localization for cooperative driving," in *2020 IEEE International Conference on Robotics and Automation (ICRA)*, 2020, pp. 1256–1262.
- [13] Q. Chen, S. Tang, Q. Yang, and S. Fu, "Cooper: Cooperative perception for connected autonomous vehicles based on 3d point clouds," in *2019 IEEE 39th International Conference on Distributed Computing Systems (ICDCS)*, 2019, pp. 514–524.
- [14] A. Geiger, P. Lenz, and R. Urtasun, "Are we ready for autonomous driving? the KITTI vision benchmark suite," in *2012 IEEE Conference on Computer Vision and Pattern Recognition*. IEEE Computer Society, 2012, pp. 3354–3361.
- [15] S. Manivasagam, S. Wang, K. Wong, W. Zeng, M. Sazanovich, S. Tan, B. Yang, W. Ma, and R. Urtasun, "LiDARsim: Realistic lidar simulation by leveraging the real world," in *2020 IEEE/CVF Conference on Computer Vision and Pattern Recognition*. Computer Vision Foundation / IEEE, 2020, pp. 11 164–11 173.
- [16] P. A. Lopez, M. Behrisch, L. Bieker-Walz, J. Erdmann, Y.-P. Flötteröd, R. Hilbrich, L. Lücken, J. Rummel, P. Wagner, and E. Wießner, "Microscopic traffic simulation using SUMO," in *21st International Conference on Intelligent Transportation Systems*. IEEE, 2018, pp. 2575–2582.
- [17] S. Shi, C. Guo, L. Jiang, Z. Wang, J. Shi, X. Wang, and H. Li, "PV-RCNN: point-voxel feature set abstraction for 3d object detection," in *2020 IEEE/CVF Conference on Computer Vision and Pattern Recognition*. Computer Vision Foundation / IEEE, 2020, pp. 10 526–10 535.
- [18] B. Graham, "Sparse 3d convolutional neural networks," in *Proceedings of the British Machine Vision Conference*. BMVA Press, 2015, pp. 150.1–150.9.
- [19] B. Graham and L. van der Maaten, "Submanifold sparse convolutional networks," *CoRR*, vol. abs/1706.01307, 2017.
- [20] W. Zheng, W. Tang, S. Chen, L. Jiang, and C. Fu, "CIA-SSD: confident iou-aware single-stage object detector from point cloud," in *Thirty-Fifth AAAI Conference on Artificial Intelligence*. AAAI Press, 2021, pp. 3555–3562.
- [21] S. Ioffe and C. Szegedy, "Batch normalization: Accelerating deep network training by reducing internal covariate shift," in *Proceedings of the 32nd International Conference on Machine Learning*, ser. JMLR Workshop and Conference Proceedings, vol. 37. JMLR.org, 2015, pp. 448–456.
- [22] N. Srivastava, G. E. Hinton, A. Krizhevsky, I. Sutskever, and R. Salakhutdinov, "Dropout: a simple way to prevent neural networks from overfitting," *J. Mach. Learn. Res.*, vol. 15, no. 1, pp. 1929–1958, 2014.
- [23] DRACO: 3d data compression. [Online]. Available: [https://github.com/draco/](https://github.com/draco)
- [24] G. Turk. PLY: Polygon File Format. [Online]. Available: <http://paulbourke.net/dataformats/ply/>
- [25] A. Dosovitskiy, G. Ros, F. Codevilla, A. M. López, and V. Koltun, "CARLA: An open urban driving simulator," in *1st Annual Conference on Robot Learning, CoRL 2017, Mountain View*, ser. Proceedings of Machine Learning Research, vol. 78. PMLR, 2017, pp. 1–16.
- [26] H. Caesar, V. Bankiti, A. H. Lang, S. Vora, V. E. Liong, Q. Xu, A. Krishnan, Y. Pan, G. Baldan, and O. Beijbom, "nuScenes: A multimodal dataset for autonomous driving," pp. 11 618–11 628, 2020.
- [27] P. Sun, H. Kretzschmar, X. Dotiwalla, A. Chouard, V. Patnaik, P. Tsui, J. Guo, Y. Zhou, Y. Chai, B. Caine, *et al.*, "Scalability in perception for autonomous driving: Waymo open dataset," in *2020 IEEE/CVF Conference on Computer Vision and Pattern Recognition*. Computer Vision Foundation / IEEE, 2020, pp. 2443–2451.
- [28] ETSI TR 103 562, "Intelligent Transport System (ITS); Vehicular Communications. Basic Set of Applications; Analysis of the Collective Perception Service (CPS); Release 2, Technical Report," 2020, accessed on 31 August 2021. [Online]. Available: [https://www.etsi.org/deliver/etsi\\_tr/103500.103599/103562/02.01.01\\_60/tr\\_103562v020101p.pdf](https://www.etsi.org/deliver/etsi_tr/103500.103599/103562/02.01.01_60/tr_103562v020101p.pdf)
- [29] F. A. Schiegg, I. Llatser, D. Bischoff, and G. Volk, "Collective perception: A safety perspective," *Sensors*, vol. 21, no. 1, 2021.